Acoustic-phonon scattering in a rectangular quantum wire

R. Mickevičius and V. Mitin
Department of Electrical and Computer Engineering, Wayne State University, Detroit, Michigan 48202
(Received 28 April 1993)

The rates of electron scattering by acoustic phonons in a rectangular quantum wire embedded into another material are calculated in the framework of the Fermi golden rule. Both intrasubband and intersubband electron scattering by acoustic phonons are considered. It has been shown that due to uncertainty of momentum conservation in quasi-one-dimensional systems the acoustic-phonon scattering becomes essentially inelastic in contrast to that in bulk materials. The acoustic-phonon scattering rate in quantum wires increases with the decrease of cross section of the wire and is much greater than that in bulk materials. It is shown that the correct treatment of inelasticity leads to a nonmonotonic dependence of the emission rate on electron energy and to the disappearance of the divergency of the acoustic-phonon scattering rate at the bottom of each subband. Therefore, the scattering time averaged over the distribution function exceeds considerably that calculated using elastic and quasielastic approaches where the scattering rate is divergent. We demonstrate that electron mobility at temperatures less than 100 K calculated within elastic or quasielastic approximations is greatly underestimated.

I. INTRODUCTION

Low-dimensional (LD) semiconductor structures are now widely recognized as a very promising basis for future technological applications. Quasi-one-dimensional (1D) quantum wires (QWI's) were expected to exhibit extremely high electron mobilities at low temperatures.[1] The point was that along with the virtual elimination of ionized impurity scattering as in quantum wells, the electron-electron scattering in QWI's is not as effective as in quantum wells.[1,2] The electron transport in long QWI's at temperatures below 100 K is controlled by acoustic-phonon scattering at low electric fields and by optical-phonon scattering at high electric fields. Phonons in LD structures recently attracted particular scientific attention due to effects of confinement and localization. There exist rather elaborated models for electron interaction with 1D confined longitudinal-optical (LO) phonons and by localized surface (interface) optical (SO) phonons in QWI's.[3–6] However, so far there is a considerable gap in the understanding of some essential aspects of 1D electron scattering by acoustic phonons. The existing models of acoustic-phonon scattering are mostly based on a large electron energy asymptote (see, e.g., Refs. 7–10) where acoustic-phonon energy is neglected. As we will see in due course this elastic approximation is valid only in bulk materials but fails in LD structures. Ridley has proposed[11,12] a method to allow for acoustic-phonon scattering inelasticity in LD structures by substituting the form factor, i.e., a function describing the momentum conservation uncertainty perpendicular to a quantum structure direction, by the sum of weighted Kronecker δ's. In this approach, further used by other authors (see, e.g., Ref. 13), some peculiarities of electron-phonon interaction are lost. This fact yields the significant error in evaluating electron mobility at low temperatures. There are just a few theoretical studies (see, e.g. Refs. 14 and 15) where acoustic-phonon scattering in quantum wells and wires is treated adequately taking into consideration strong inelasticity caused by momentum conservation uncertainty (*quasiconservation*). These studies, however, are restricted to quasiequilibrium electron gas and to an extreme quantum limit where only one lowest subband is populated. The intersubband transitions due to acoustic-phonon scattering, which are even more inelastic, have not yet been considered correctly.

We present results of calculations of electron scattering by acoustic phonons in a rectangular QWI where we consider inelasticity of this scattering in full detail. In Sec. II we give the basic equations of the model and derive the form factor for the electron interaction with acoustic phonons. In Sec. III various simplified as well as accurate approaches for the scattering rates are presented and compared. The low field electron mobility is calculated in Sec. III for different approximations of acoustic-phonon scattering. Section IV summarizes results obtained in the present paper.

II. BASIC APPROACH

The rate of electron scattering from the state $\mathbf{k}$ to the state $\mathbf{k}'$, with the assistance of a phonon with wave vector $\mathbf{q}$ is given by the Fermi golden rule,

$$W(\mathbf{k},\mathbf{k}',\mathbf{q})=\frac{2\pi}{\hbar}|\langle\Phi'\varphi_{k'}|H|\Phi\varphi_k\rangle|^2 \times\delta(\epsilon_k-\epsilon_{k'}-\Delta\epsilon\mp\hbar\omega_q)\,, \quad (1)$$

where Φ is the phonon wave function and φ is the electron wave function, the prime denotes the state after the scattering event, the δ function represents energy conservation, and $\Delta\epsilon$ is the energy separation between initial (j,l) and final (j',l') subbands. Here and everywhere below the upper sign corresponds to emission and the lower sign to absorption of the acoustic phonon. Within the approach of the deformation potential the above ex-

pression turns into

$$W(\mathbf{k},\mathbf{k}',\mathbf{q})=\frac{2\pi}{\hbar}(N_q+\tfrac{1}{2}\pm\tfrac{1}{2})|H(q)|^2|I|^2 \times\delta(\epsilon_k-\epsilon_{k'}-\Delta\epsilon\mp\hbar\omega_q)\ , \quad (2)$$

where

$$|H(q)|^2=\frac{\hbar E_a^2 q^2}{2\rho V\omega_q}\ , \quad (3)$$

V is the principal volume of the crystal, E_a^2 is the deformation acoustic potential, ρ is the density of the materials, $\omega_q=uq$ is the long wave approximation of acoustic-phonon dispersion, where u is a sound velocity in the material, and I in (2) is an overlap integral:

$$I=\langle\varphi_{k'}|e^{i\mathbf{q}\cdot\mathbf{r}}|\varphi_k\rangle\ . \quad (4)$$

We will consider here a rectangular quantum wire with an infinitely deep potential well in both perpendicular directions (y and z) so that the electron wave function is given by

$$|\varphi_k\rangle=\left[\frac{1}{L_x}\right]^{1/2}e^{ik_x x}\left[\frac{2}{L_y}\right]^{1/2} \times\sin\left[\frac{j\pi y}{L_y}\right]\left[\frac{2}{L_z}\right]^{1/2}\sin\left[\frac{l\pi z}{L_z}\right]\ , \quad 0\le y\le L_y,\ 0\le z\le L_z\ , \quad (5)$$

where j and l are subband indices in y and z quantized directions, respectively. The electron kinetic energy and the energy separation between subbands are given by

$$\epsilon_{k_x}=\frac{\hbar^2k_x^2}{2m^*}\ , \quad (6)$$

$$\Delta\epsilon=\frac{\hbar^2}{2m^*}\left[\left[\frac{\pi}{L_y}\right]^2(j'^2-j^2)+\left[\frac{\pi}{L_z}\right]^2(l'^2-l^2)\right]\ . \quad (7)$$

Integrating over the volume of the quantum wire and neglecting umklapp processes we get

$$|I|^2=G\times\delta_{k_x\mp q_x,k_x'}\ ,$$

$$G=\frac{2[(2\pi)^2q_yL_yjj']^2[1-(-1)^{j+j'}\cos(q_yL_y)]}{[(q_yL_y)^4-2\pi^2(q_yL_y)^2(j^2+j'^2)+\pi^4(j^2-j'^2)^2]^2} \times\frac{2[(2\pi)^2q_zL_zll']^2[1-(-1)^{l+l'}\cos(q_zL_z)]}{[(q_zL_z)^4-2\pi^2(q_zL_z)^2(l^2+l'^2)+\pi^4(l^2-l'^2)^2]^2}\ . \quad (8)$$

The overlap integral I contains the Kronecker δ which reflects momentum conservation in the x direction. Due to the lack of translational symmetry in the y and z directions, the form factor G deviates considerably from the double Kronecker δ which is relevant to bulk materials. This deviation is responsible for the uncertainty of momentum conservation (quasiconservation) in the y and z directions. Roughly speaking the half-width of G determines this uncertainty. To get an idea of how large this uncertainty is we have to analyze the detailed structure of the form factor. The form factor has its main maxima at

$$q_yL_y=\pm\pi(j\pm j'),\quad q_zL_z=\pm\pi(l\pm l') \quad (9)$$

and a number of subsidiary maxima which are several orders of magnitude lower than the main maxima and are not as important as the main maxima. For intrasubband electron scattering ($j=j'$ and $l=l'$) the form factor has the absolute maximum $G=1$ at $q_y=0,q_z=0$. For rough estimates we may assume that the position of the second maximum (sign plus) defines the uncertainty of momentum conservation and is responsible for additional inelasticity of electron scattering by acoustic phonons in QWI's. Obviously, we have stronger inelasticity for electron scattering between higher subbands and in thinner wires. As sizes of the quantum wire L_y and L_z turn to infinity, the form factor G turns into a double Kronecker δ.

The dependences of the form factor on one component of the phonon wave vector are presented in Fig. 1 for several intrasubband and intersubband transitions. As one can see from Fig. 1 the two maxima of the form factor overlap for the transitions inside the first subband as well as between the first subband and upper subbands forming a broader peak. The point is that positions of the first and the second maxima $j'-1$ and $j'+1$, respectively, are close to each other. The region between two indistinguishable maxima contributes essentially to the scattering rate and cannot be ignored as it has been done in Ref. 11. The complete three dimensional plot of G as a function of q_y and q_z is very complicated since it consists of many peaks: one for each single set of q_y and q_z given by Eq. (9).

Substituting I back into Eq. (2) we can find the scattering rate from the state k_x of subband (j,l) to any state of

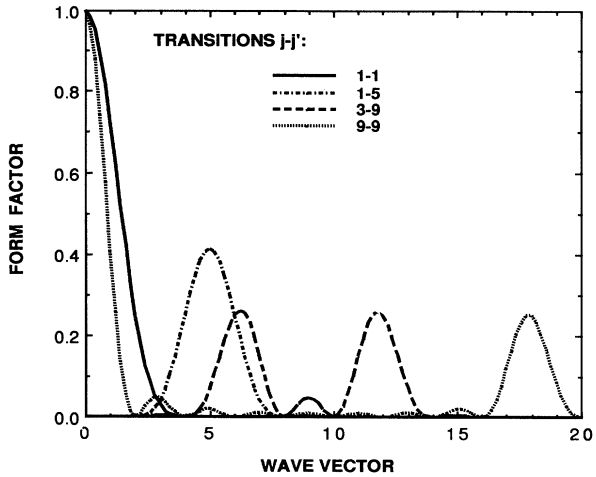

FIG. 1. The form factor G as a function of the normalized transverse component of phonon wave vector q_yL_y/π. Another transverse component q_z is set to be zero. The numbers in the legend represent different intrasubband or intersubband transitions, e.g., 1-1 means transitions from the subband $j=1$ to the subband $j'=1$, etc.

subband (j',l'),

$$\lambda(k_x)=\frac{V}{(2\pi)^3}\sum_{k_x'}\int d\mathbf{q}W(k_x,k_x',\mathbf{q}) . \tag{10}$$

The above equation after the summation over k_x' turns into

$$\lambda(k_x)=\frac{E_a^2}{8\pi^2\rho u}\int dq_x dq_y dq_z (q_x^2+q_y^2+q_z^2)^{1/2} \times G(N_q+\tfrac{1}{2}\pm\tfrac{1}{2}) \times\delta[\epsilon_{k_x}-\epsilon_{k_x\mp q_x}-\Delta\epsilon \mp\hbar u(q_x^2+q_y^2+q_z^2)^{1/2}] . \tag{11}$$

This is a basic equation for the calculation of the scattering rates. The complexity of the form factor does not allow one to get analytical results without certain simplifications. In the next section we introduce some simplifications permitting us to analyze asymptotic behavior of the scattering rates. We will present (Appendix B) exact numerical integration of Eq. (11) as well.

III. SCATTERING RATES AND LOW-FIELD ELECTRON MOBILITY

We will consider a QWI embedded into another material with similar elastic properties so that acoustic phonons can penetrate through the interface between these materials. Due to different sound velocities in these materials the acoustic wave will refract (change its wavelength) while penetrating and will adjust to a new environment. That is why all parameters are taken from the first material (quantum wire). Some corrections due to partial reflection of the acoustic wave should be considered in a more elaborated approach. For all numerical calculations we use parameters of GaAs QWI's supposedly embedded in $Al_xGa_{1-x}As$. As we deal with 1D structures it is convenient to separate the scattering back (electron wave vector changes its sign to the opposite during the scattering event) and the scattering forth (electron wave vector does not change its sign). In some cases, however, when dealing with the different approximations we will compare the total scattering rates which are sums of the forward and backward scattering rates.

Let us first obtain somewhat simplified but analytically transparent results. We assume that phonon energy $\hbar uq \ll k_BT$. Then

$$N_q\approx N_q+1\approx\frac{k_BT}{\hbar uq}\gg 1 . \tag{12}$$

The second assumption is that $q_x \ll q_T$, where $q_T=\sqrt{q_y^2+q_z^2}$ is a transverse component of the phonon wave vector. This assumption is valid for a wide range of electron energies (see Appendix A). Within this assumption we may neglect the q_x component in the phonon energy.

To meet both above assumptions it is required that

$$\hbar uq_{T\max}\ll k_BT , \tag{13}$$

where

$$q_{T\max}=\pi\left[\left[\frac{j+j'}{L_y}\right]^2+\left[\frac{l+l'}{L_z}\right]^2\right]^{1/2} \tag{14}$$

is roughly the maximum transverse component of the phonon wave vector. For GaAs 250×150 Å QWI's and transitions in the first subband $(j=j'=l=l'=1)$ the inequality (13) is satisfied roughly for $T\gg 15$ K. This phonon wave vector coincides with the position of one of the main maxima of G.

Then integrating (11) over q_x we get

$$\lambda(\epsilon)=\frac{E_a^2k_BT}{4\pi^2\rho u^2\hbar^2}\left[\frac{m^*}{2}\right]^{1/2}\int\frac{dq_ydq_zG}{\sqrt{\epsilon\mp\hbar uq_T-\Delta\epsilon}} . \tag{15}$$

The integration limits for the absorption rate are imposed by the form factor which tends to zero above $q_{T\max}$. As the electron energy tends to zero the absorption rate saturates since $q_{T\max}$ is not equal to zero. This is in contrast to the elastic and quasielastic approximations where absorption and emission rates diverge as one-over-square-root of electron energy.

For the emission rate let us consider two asymptotic cases of (i) very small and (ii) very large electron energies ϵ.

(i) $\epsilon\ll\hbar uq_{T\max}$. In this case we will consider only intrasubband scattering $\Delta\epsilon=0$. The limits of integration of (15) for the emission rate are imposed in this case by the requirement that the expression under the square root is positive, i.e., $\hbar uq_T\le\epsilon\ll\hbar uq_{T\max}$. In this range of $q_T\ll q_{T\max}$ the form factor G is close to its first maximum value equal to 1 and weakly depends on the phonon wave vector. Therefore, we have taken $G=1$ for qualitative estimates. Then Eq. (15) can be simplified to

$$\lambda(\epsilon)=\frac{2E_a^2k_BT}{3\pi\rho u^4\hbar^4}\left[\frac{m^*}{2}\right]^{1/2}\epsilon^{3/2} . \tag{16}$$

As one can see from (16) the emission rate increases as a 3/2 power of electron energy and does not depend on the thickness of a QWI. The emission rate goes to zero as electron energy approaches zero. (In a more elaborated approach where the q_x component is not neglected the forward emission rate turns to zero for electron energy $\epsilon<m^*u^2/2$ and backward emission rate for $\epsilon<2m^*u^2$.) Physically it corresponds to the reduction of the final states for the scattered electron.

(ii) $\epsilon-\Delta\epsilon\gg\hbar uq_{T\max}$. In this case we may neglect phonon energy (the expression under the square root is always positive within the range of nonzero form factor G). Note that for this asymptote emission and absorption rates are equal. Then (15) turns into

$$\lambda(\epsilon)=\frac{E_a^2k_BT}{\rho u^2\hbar^2L_yL_z}\left[\frac{m^*}{2(\epsilon-\Delta\epsilon)}\right]^{1/2}(1+\tfrac{1}{2}\delta_{jj'})(1+\tfrac{1}{2}\delta_{ll'}) . \tag{17}$$

Thus the high-energy asymptote is a one-over-square-root function of electron kinetic energy after scattering, the same as the 1D density of states function. This suggests

that there is a maximum emission rate in the intermediate energy region.

Figure 2 demonstrates the scattering rates in the first subband versus electron energy for GaAs QWI's calculated with Eq. (15). For comparison we also plot the exact scattering rates obtained without any simplifications of Eq. (11). The details of numerical calculation of the integral (11) are given in Appendix B. The coincidence between results obtained within exact (11) and simplified (15) models is rather good. The discrepancy primarily stems from approximation (12) which is not accurate enough at such low temperatures as $T=30$ K. (This leads to an essential difference between emission and absorption rates.) The qualitative behavior, however, is in excellent agreement. The emission rate has its maximum at the electron energy corresponding to the transition from low energy asymptote to high energy asymptote, which can be roughly estimated as $\epsilon_c=\hbar u q_{T\max}$ with $q_{T\max}$ given by (14). Since $q_{T\max}\propto 1/L$, where L is the effective thickness of the quantum wire $L^{-2}=L_y^{-2}+L_z^{-2}$, the maximum emission energy ϵ_c increases as the QWI thickness decreases. This is illustrated in Fig. 3, where the scattering rate for two QWI sizes is plotted against electron energy. Note that these scattering rates are calculated by direct numerical integration of (11) without further simplifications and forward and backward scattering rates are plotted separately. Well below the maximum emission energy ϵ_c the emission does not depend on QWI size as it has been pointed out above. The maximum emission rate and the rate above the maximum (as well as the absorption rate) increase as the thickness of a quantum wire decreases. One can see that the rates of backward and forward scattering coincide in a wide energy region.

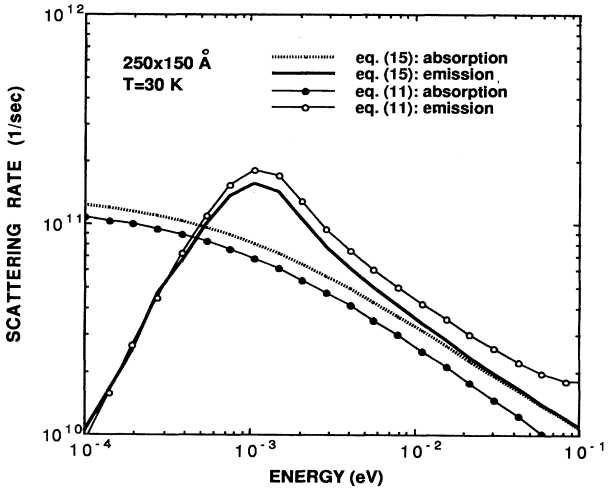

FIG. 2. The total acoustic-phonon emission and absorption rates (backward+forward) versus electron energy for the transitions in the lowest subband. Curves with circles represent results of exact numerical integration of Eq. (11); the other two curves (solid and dotted) represent simplified results given by Eq. (15). The GaAs/AlAs QWI with cross section 250×150 Å^2, lattice temperature $T=30$ K.

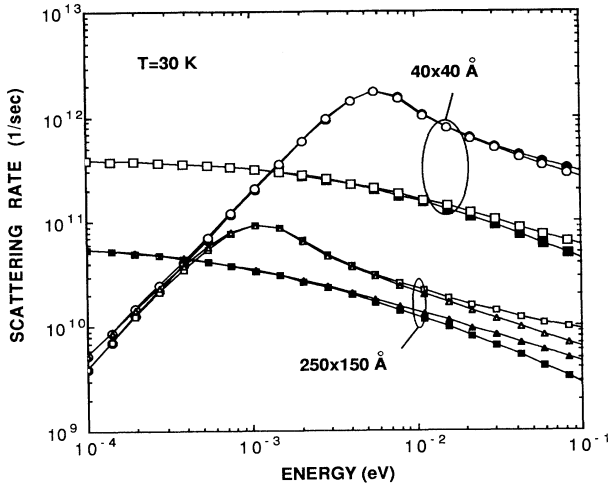

FIG. 3. Acoustic-phonon scattering rates in the lowest subband calculated from Eq. (11) versus electron energy for two cross sections of the QWI. Backward and forward scattering rates are plotted separately. For notation see Fig. 5. $T=30$ K.

The high-energy asymptote given by Eq. (17) is frequently extended to a low-energy region (see, e.g., Refs. 7–9 and 13) ignoring the fact that inequality $\epsilon-\Delta\epsilon\gg\hbar u q_{T\max}$ no longer holds. This, the so-called *elastic approximation,* yields equal emission and absorption rates and divergency of these rates as ϵ tends to zero. The elastic approximation cannot be justified for the transport calculations at low temperatures, i.e., exactly where acoustic-phonon scattering plays a decisive role. The point is that at low temperatures a vast majority of electrons are accumulated close to the subband bottom where the elastic approximation leads to the overestimated scattering rates.

In the *momentum conservation* or *quasielastic* approach of Ref. 11 the substitute for the form factor G is used in the form of the sum of the weighted Kronecker δ's,

$$G\propto\left[\sum_n\delta_{q_y,q_{yn}}+2\delta_{q_y,0}\delta_{j,j'}\right]\left[\sum_m\delta_{q_z,q_{zm}}+2\delta_{q_z,0}\delta_{l,l'}\right],$$

where q_{yn} and q_{zm} are the positions of the nth and mth maxima given by Eq. (9). This approximation neglects the smooth shape of the form factor responsible for the uncertainty of momentum conservation. The inelasticity of acoustic-phonon scattering within this approximation stems from δ's corresponding to the upper maxima of the form factor. The major contribution to the scattering rate, however, comes from the first δ function corresponding to the maximum of G at $q_y=q_z=0$, i.e., from the elastic term in the expansion of the form factor. For $l=l'$ the maximum corresponding to $q_z=0$ comes into the sum four times, while the secondary maximum $q_z\neq0$ comes only twice. Consequently, the major contribution to the intrasubband scattering rate comes from the acoustic phonons with zero transverse components of their wave vector. Substituting the above approximation for G

in (15) one gets

$$\lambda(\epsilon)=\frac{E_a^2 k_B T}{4\rho u^2 \hbar^2 L_y L_z}\left[\frac{m^*}{2}\right]^{1/2}\sum_i \frac{\Theta(\epsilon\mp\hbar u q_{Ti}-\Delta\epsilon)}{\sqrt{(\epsilon\mp\hbar u q_{Ti}-\Delta\epsilon)}}\ , \tag{18}$$

where the index i runs over all major maxima (9) of the form factor in the non-negative quarter of the $q_y q_z$ plane. This means that terms corresponding to zero q_y or q_z appear twice and terms corresponding to both q_y and q_z equal to zero appear four times in the above sum. It is evident from (18) that both emission (sign minus) and absorption (sign plus) rates diverge at $\epsilon=0$ for intrasubband transitions. In addition to this divergency the emission rate diverges at each electron energy corresponding to the maximum of the form factor. The scattering rate within this quasielastic approach, like the elastic approximation, is inversely proportional to a QWI cross section $L_y \times L_z$ and diverges as the cross section approaches zero. The inelastic approach avoids this divergency since the maximum acoustic phonon energy at the edge of the Brillouin zone sets the limits for integration over phonon wave vector in Eq. (11) (see Appendix B).

Figure 4 demonstrates the differences between the scattering rate dependencies on electron energy calculated within inelastic, quasielastic, and elastic models. One can see that for the quasielastic approximation the emission and absorption rates differ significantly only in the intermediate energy region and coincide at low and large energies. Some difference between emission and absorption rates, particularly at low temperatures, would occur if the approximation (12) was not used. At high temperatures, where approximation (12) holds, this difference would be negligible. The same apply to the elastic approximation. The correct inelastic treatment of acoustic-phonon scattering, however, yields qualitatively different scattering rates. Emission and absorption rates within the latter approach are always considerably different at low energies independent of lattice temperature. There is no divergency of the scattering rates within the inelastic approach unlike divergencies that are inherent to elastic and quasielastic models. Due to divergencies of the scattering rates for elastic and quasielastic approximations, the scattering rate averaged over the distribution function is substantially overestimated.

The scattering rates for transitions between the upper subbands we calculated by direct integration of (11) without any simplifications. The rates of electron scattering in the upper subbands are presented in Fig. 5. One

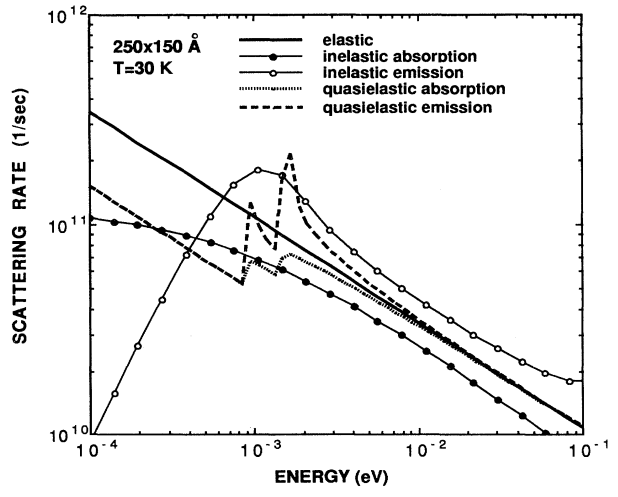

FIG. 4. Energy dependencies of the acoustic-phonon scattering rates obtained within different approaches: elastic from Eq. (17), quasielastic from Eq. (18), and inelastic from Eq. (11). The total rates plotted (backward+forward) are for transitions within the lowest subband of the 250×150 Å^2 QWI at $T=30$ K. Note that the maxima on the quasielastic emission rate in fact are divergent.

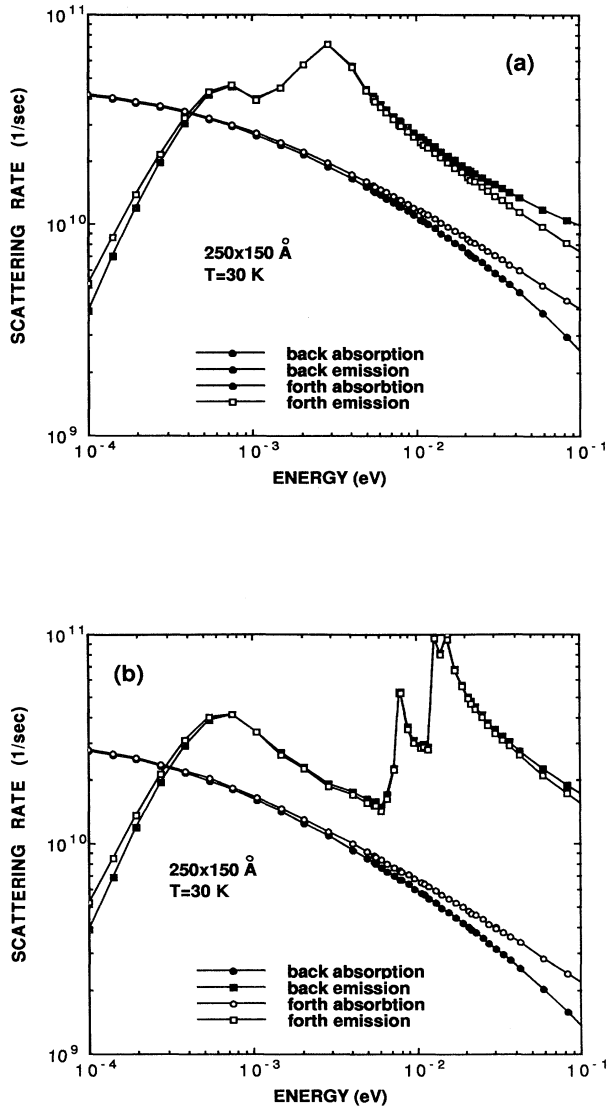

FIG. 5. The rates of scattering within the upper subbands: (a) within the subband (2,2): $J=2, l=2$, (b) within the subband (9,9): $j=9, l=9$. Forward and backward scatterings are plotted separately. QWI sizes 250×150 Å^2, $T=30$ K.

can see additional distinguishable peaks caused by the secondary maxima of the form factor on the emission rates inside the upper subbands. The secondary maxima, corresponding to at least one nonzero component of phonon wave vector q_y or q_z, contribute to the absorption and emission rates in essentially different ways. Any electron, regardless of its energy, can absorb a phonon with arbitrarily large energy and with an arbitrarily large transverse component of phonon wave vector. Therefore, the secondary maxima of the form factor, corresponding to large phonon energies, contribute to the absorption rate for all electron energies. The situation is completely different with the emission processes. An electron can emit only those phonons that have energy less than its own energy. Consequently, the upper maximum of the form factor cannot contribute to the emission rate if the electron energy is less than the energy of the phonon corresponding to that particular maximum. This is why the emission rate can increase sharply as the electron energy reaches the energy of the acoustic phonon corresponding to the upper maximum of the form factor. One can see three distinguishable peaks that form the fine structure for the transitions where subband indices before and after scattering j,j' and l,l' are considerably greater than 1 [see Fig. 5(b) for the transition in the subband (9,9)], because the maxima of the form factor are well separated (see Fig. 1). Each peak corresponds to a maximum of the form factor. There are three peaks because the form factor is a two-dimensional function and it has several maxima in the $q_y q_z$ plane that correspond to *different phonon energies* (since $L_y \neq L_z$). When subband indices are close to 1 [see the emission rate for transitions in subband (2,2) in Fig. 5(a)] all these peaks caused by the secondary maxima of the form factor are not distinguishable; they turn into one broad maximum.

In order to compare physical consequences of different approaches to acoustic-phonon scattering we have calculated low field electron mobility using probe particle

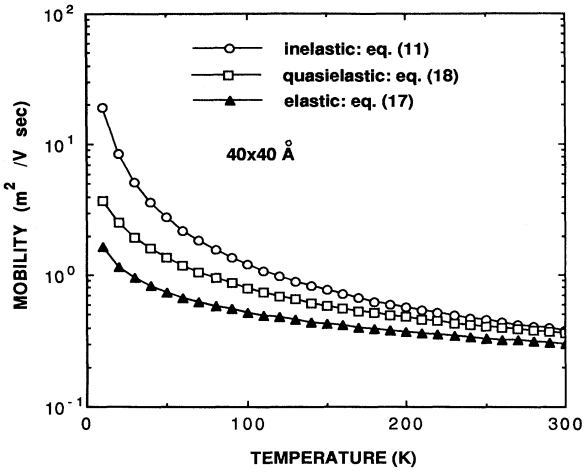

FIG. 6. Low-field electron mobility as a function of temperature. Various curves represent different approaches: inelastic Eq. (11), quasielastic Eq. (18), elastic Eq. (17). QWI sizes 40×40 Å^2.

method: $\mu = e/m^*\langle\tau\rangle$, where $\langle\tau\rangle$ is the momentum relaxation time due to acoustic-phonon scattering averaged over the equilibrium electron distribution function. The mobility is plotted versus temperature in Fig. 6. As one can see, electron mobility calculated within elastic and quasielastic approaches is significantly underestimated in the low temperature region. The mobility calculated within an accurate inelastic approach is higher by an order of magnitude than "elastic" mobility at $T=10$ K. The quasielastic approach of Refs. 11 and 12 leads to close agreement with the inelastic approach at higher temperatures but still the mobility below $T=100$ K differs significantly. The reason for this is obvious: an overestimation of the acoustic-phonon scattering rate (especially emission rate) at the low energy region. Since elastic and quasielastic models both do not avoid divergency of the scattering rate, these divergency points and their vicinity contribute greatly to the total scattering rate averaged over the distribution function (in other words, they contribute negligibly to the average scattering time). Moreover, even without divergency the emission rate is far overestimated in the low-energy region (see Fig. 4) and thus leads to underestimated electron mobilities at low temperatures. It is worthwhile to stress again that mobility decreases as the cross section of the quantum wire decreases.

IV. SUMMARY AND DISCUSSION

We have calculated 1D electron scattering rates by acoustic phonons in a rectangular quantum wire in the framework of the Fermi golden rule. The calculated rates are suitable for direct incorporation into Monte Carlo codes (because forward and backward scattering processes are treated separately). Our investigation has shown that many details of the electron scattering usually omitted in previous works come into effect in low dimensional structures and should be taken into account. The elasticity of electron–acoustic-phonon scattering is a commonly used approximation.[7,13] A closer look at this mechanism of scattering shows that electron scattering by acoustic phonons in quantum wires becomes essentially inelastic. This is due to the fact that the momentum conservation for electron–acoustic-phonon systems is preserved only with an accuracy of $2\pi\hbar/L$, where $L^{-2}=L_y^{-2}+L_z^{-2}$. For a GaAs quantum wire with $L_y=L_z=40$ Å the electron energy corresponding to momentum $2\pi\hbar/L$ is approximately equal to 7 meV, i.e., corresponding to 1D electron temperature over 100 K. So in a wide range of system parameters an electron can absorb or emit an acoustic phonon with energy comparable with its own energy. That means the electron–acoustic-phonon scattering turns out to be essentially inelastic and becomes an effective mechanism of energy dissipation. Moreover, the momentum conservation for electron transitions in between upper subbands is satisfied even with lower accuracy. This results in even higher inelasticity of electron–acoustic-phonon scattering so that the long-wave approximation for acoustic-phonon scattering breaks down. The total rate of acoustic-phonon scattering differs considerably from

$\epsilon^{-1/2}$ (where ϵ is the electron kinetic energy after scattering) function obtained in Refs. 7 and 13. The real energy dependence of the scattering rate is determined by details of the overlap integral and can have very complex structure. The complex nature of the overlap integral is responsible for a fine structure of the scattering rate for transitions in upper subbands of a quantum wire.

Low-field electron mobility at low lattice temperatures calculated within the accurate inelastic approach exceeds significantly the mobility calculated within elastic and quasielastic approximations.

We have used a somewhat simplified model of infinitely high potential barriers for electrons. For a finite height of barriers the electron wave function extends into the barrier regions. Therefore, the effect of finite height barriers is analogous to the increase of the effective thickness of a QWI and should not be strong in GaAs/AlAs structures.

ACKNOWLEDGMENTS

The authors thank N. Bannov for useful discussions. This work was supported by the NSF and by ARO under Grant No. DAAL03-92-G0044.

APPENDIX A: RELATIONSHIP BETWEEN PARALLEL AND PERPENDICULAR COMPONENTS OF THE PHONON WAVE VECTOR

From energy conservation it follows that

$$q_x^2\left[\left[\frac{\hbar}{2m^*u}\right]^2(q_x\mp 2k_x)^2-1\right]=q_T^2 \ . \tag{A1}$$

The factor in square brackets on the left-hand side of the above equation is much larger than 1 if

$$\frac{\hbar^2(q_x\mp 2k_x)^2}{2m^*}\gg m^*u^2 \ . \tag{A2}$$

By substituting numerical values for GaAs one can see that the above inequality holds for electron energies higher than 0.01 meV.

APPENDIX B: EXACT NUMERICAL CALCULATION OF THE ACOUSTIC-PHONON SCATTERING RATES

If we do not neglect parallel components of phonon wave vector q_x in the expression for phonon energy, the most convenient way to proceed with numerical integration of Eq. (11) is to integrate it first over one of the transverse components, say q_z. This integration leads to

$$\lambda(k_x)=\int_{q_{x\,\min}}^{q_{x\,\max}}dq_x F(q_x) \ ,$$

$$F(q_x)=\frac{E_a^2}{2\pi^2\rho u^2\hbar}\left[\frac{\epsilon_{k_x}-\epsilon_{k_x\mp q_x}-\Delta\epsilon}{\hbar u}\right]^2 \times\int_{q_{y\,\min}}^{q_{x\,\max}}dq_y G(N_q+\tfrac{1}{2}\pm\tfrac{1}{2}) \times\left[\left[\frac{\epsilon_{k_x}-\epsilon_{k_x\mp q_x}-\Delta\epsilon}{\hbar u}\right]^2-q_x^2-q_y^2\right]^{-1/2} . \tag{B1}$$

In Eq. (11) q_z is substituted by

$$q_z=\left[\left[\frac{\epsilon_{k_x}-\epsilon_{k_x\mp q_x}-\Delta\epsilon}{\hbar u}\right]^2-q_x^2-q_y^2\right]^{1/2} , \tag{B2}$$

which follows from energy conservation (integration over q_z of the δ function).

Function $F(q_x)$ defines the nonelasticity of acoustic scattering (q_x is uniquely related to phonon energy $\hbar\omega$) and is used to randomly choose the electron final state after acoustic scattering.

Unlike the form factor, the function F has its maximum shifted up from zero. This is due to the fact that accurate treatment of inelasticity gives rise to an additional factor before the scattering rate proportional to q_x^2, i.e., it forbids transitions with $q_x=0$ (i.e., elastic with zero phonon energy). Note that the maximum point is defined solely by the form factor, i.e., by the QWI thickness. For backward scattering we have threshold phonon energy (defined by momentum conservation) and almost all backscattering is assisted by acoustic phonons which have energy equal to or just above this threshold ($q_T=0$) for high energetic electrons. For lower electron energies backward electron scattering has a peak at the same phonon energy as forward scattering since the threshold phonon energy is below this maximum point.

The limits of integration are imposed by energy conservation (the requirement that the expression under the square root is greater than zero). It is convenient to consider backward and forward scattering separately in quantum wires. The point is that this form is well suited for direct incorporation into Monte Carlo codes. Moreover, it is important to distinguish between forward and backward scattering by acoustic phonons as backward scattering plays a far more important role in electron momentum relaxation and defining transport parameters. Then the limits of integration in the above equations are defined by

$$q_{x\min}=-k_x-\mathrm{sgn}(\Delta\epsilon)\frac{m^*u}{\hbar}+\left[\left[k_x+\mathrm{sgn}(\Delta\epsilon)\frac{m^*u}{\hbar}\right]^2-\frac{2m^*\Delta\epsilon}{\hbar^2}\right]^{1/2} ,$$

$q_{x\max}=\infty$ for forward absorption;

$$q_{x\min}=k_x-\mathrm{sgn}(\Delta\epsilon)\frac{m^*u}{\hbar}-\left[\left[k_x-\mathrm{sgn}(\Delta\epsilon)\frac{m^*u}{\hbar}\right]^2-\frac{2m^*\Delta\epsilon}{\hbar^2}\right]^{1/2} ,$$

$$
\begin{aligned}
&q_{x\max}=k_x \quad \text{for forward emission;} \\
&q_{x\max}=-k_x-\frac{m^*u}{\hbar}+\left[\left[k_x+\frac{m^*u}{\hbar}\right]^2-\frac{2m^*\Delta\epsilon}{\hbar^2}\right]^{1/2}, \\
&q_{x\min}=-\infty \quad \text{for backward absorption;} \\
&q_{x\max}=k_x-\frac{m^*u}{\hbar}+\left[\left[k_x-\frac{m^*u}{\hbar}\right]^2-\frac{2m^*\Delta\epsilon}{\hbar^2}\right]^{1/2}, \\
&q_{x\min}=k_x \quad \text{for backward emission.}
\end{aligned}
\tag{B3}
$$

Here the sgn function is equal to $+1$ if $\Delta\epsilon=0$. The above limits are for the case when electron kinetic energy in subband (j,l) is greater than $\Delta\epsilon$. In the opposite case emission is impossible and for absorption we have $q_{x\min}=-k_x$. If the upper limit in (B3) is less than the lower limit (as it can be in the case of emission), the scattering rate is equal to zero.

For all above cases the limits of integration over q_y are given by

$$
\begin{aligned}
&q_{y\max}^2=\frac{1}{\hbar^2u^2}\left[\frac{\hbar^2q_x^2}{2m^*}\mp\frac{\hbar^2q_xk_x}{m^*}+\Delta\epsilon\right]^2-q_x^2, \\
&q_{y\min}^2=0 .
\end{aligned}
\tag{B4}
$$

The additional restrictions for integration limits are imposed by $q_{y\max}^2>0$ and the requirement that acoustic-phonon energy is less than that at the edge of the Brillouin zone. The latter restriction, however, may be ignored since the contribution of acoustic phonons with energies of the order of optical phonon energy is negligible. In the case of intrasubband scattering the above limits turn to a simple form:

$$
\begin{aligned}
&q_{x\min}=0, \quad q_{x\max}=\infty \quad \text{for forward absorption;} \\
&q_{x\min}=0, \quad q_{x\max}=k_x \quad \text{for forward emission;} \\
&q_{x\min}=-\infty, \quad q_{x\max}=-2k_x-2m^*u/\hbar \quad \text{for backward absorption;} \\
&q_{x\min}=k_x, \quad q_{x\max}=2k_x-2m^*u/\hbar \quad \text{for backward emission .}
\end{aligned}
\tag{B5}
$$

The limits of integration over q_y are now given by

$$
\begin{aligned}
&q_{y\max}^2=\frac{\hbar^2q_x^2}{2m^*}\frac{(q_x\mp2k_x)^2}{2m^*u^2}-q_x^2, \\
&q_{y\min}^2=0 .
\end{aligned}
\tag{B6}
$$

The integral for scattering rate (B1) has been taken numerically. There are, however, extraordinary points (limits of internal and external integrals) where the function under the internal integral (over q_y) diverges. The vicinity of these points has been integrated analytically.

[1]H. Sakaki, Jpn. J. Appl. Phys. **19**, L735 (1980).

[2]G. Fasol and H. Sakaki, in the *2nd International Symposium on New Phenomena in Mesoscopic Structures, Hawaii, 1992,* edited by T. Ando and C. Hamaguchi (Osaka University, Maui, 1992), p. 335.

[3]N. Mori and T. Ando, Phys. Rev. B **40**, 6175 (1989).

[4]R. Mickevičius, V. V. Mitin, K. W. Kim, and M. A. Stroscio, Semicond. Sci. Technol. **7**, B299 (1992).

[5]H. Rücker, E. Molinari, and P. Lugli, Phys. Rev. B **44**, 3463 (1991).

[6]P. A. Knipp and T. L. Reinecke, Phys. Rev. B **45**, 9091 (1992).

[7]F. Comas, C. Trallero Giner, and J. Tutor, Phys. Status Solidi B **139**, 433 (1987).

[8]V. K. Arora and M. Prasad, Phys. Status Solidi B **117**, 127 (1983).

[9]V. K. Arora and A. Naeem, Phys. Rev. B **31**, 3887 (1985).

[10]M. P. Chamberlain, D. Hoare, R. W. Kelsall, and R. A. Abram, Semicond. Sci. Technol. **7**, B45 (1992).

[11]B. K. Ridley, J. Phys. C **15**, 5899 (1982).

[12]B. K. Ridley, Rep. Prog. Phys. **54**, 169 (1991).

[13]J. Lee and M. O. Vassell, J. Phys. C **17**, 2525 (1984).

[14]V. Karpus, Fiz. Tekh. Poluprovodn. **20**, 12 (1986) [Sov. Phys. Semicond. **20**, 6 (1986)].

[15]A. Kabasi, D. Chattopadhay, and C. K. Sarkar, J. Appl. Phys. **65**, 1598 (1989).